

Quasiperiodicity protects quantized transport in disordered systems without gaps

Emmanuel Gottlob,^{1,*} Dan S. Borgnia,^{2,†} Robert-Jan Slager,^{3,‡} and Ulrich Schneider^{1,§}

¹*Cavendish Laboratory, University of Cambridge,
JJ Thomson Avenue, Cambridge CB3 0HE, United Kingdom*

²*Department of Physics, University of California, Berkeley, California 94720, USA*

³*TCM Group, Cavendish Laboratory, Department of Physics,
JJ Thomson Avenue, Cambridge CB3 0HE, United Kingdom*

(Dated: July 10, 2024)

The robustness of topological properties, such as adiabatic quantized currents, generally depends on the existence of gaps surrounding the relevant energy levels or on symmetry-forbidden transitions. We uncover a new mechanism for topological protection via the observation of quantized currents that survive the addition of bounded local disorder beyond the closing of the relevant instantaneous energy gaps in a driven Aubry-André-Harper chain, a prototypical model of quasiperiodic systems. Using a local picture in *configuration-space* based on Landau-Zener transitions, we show that in this case the topological protection does not depend on the spectral gaps, but rather on the number of states in an occupied band and the position of the band in configuration space. Moreover, we propose a protocol, directly realizable in for instance cold atoms or photonic experiments, which leverages this stability to prepare topological many-body states with high Chern numbers and opens new experimental avenues for the study of both the integer and fractional quantum Hall effects.

A key feature of topological phases is the robustness to local perturbations that leads to quantized physical observables characterized by a bulk topological invariant, a famous example of which is found in the integer quantum Hall effect [1, 2]. Topological phases can also be realised in dynamical systems, where time is interpreted as an additional *virtual* dimension. The canonical example is Thouless pumping [3, 4], where slow time-periodic modulation of a typically 1D Hamiltonian generates quantized charge transport indexed by *virtual* 2D Chern numbers [5, 6]. Experimentally, Thouless pumps have been realized within various platforms, e.g. photonic waveguides [7] or ultracold atoms [8–11]. They are typically considered in the context of periodic systems, where the pumped charge is only quantised when the pumping time is an exact multiple of the pump period. In contrast, Thouless pumping in *quasiperiodic* systems can exhibit constant quantized pumped charge and currents at all times during the pump cycle [12].

The stability of quantized Thouless pumping to disorder remains a topic of active research [4, 13, 14]. More generally, it has long been shown mathematically that the adiabatic theorem does not require a spectral gap [15], even in open quantum systems [16]. For experimentally accessible observables such as the pumped charge, on the other hand, topological quantisation typically remains stable to generic perturbations only up to the closing of spectral gaps or mobility gaps – gaps between delocalized eigenstates [17] – and/or the breaking of explicit symmetry protections [18–21]. In particular, it was shown that Thouless pumps in periodic systems break down under

closing of the energy gaps by disorder [22–24]. In this letter, we report on an experimentally accessible Thouless pump for quasiperiodic systems, characterized by persistent quantized pumping in the presence of large bounded local disorder, surviving the disorder-induced closure of spectral gaps. The topological protection does not rest on any spectral condition or symmetry protection and instead depends on the number of states in the pumped band, in stark contrast with previously known examples.

To explain this counter-intuitive robustness, we develop a perturbative argument based on local Landau-Zener (avoided-crossing) transitions, and derive analytical expressions for the critical disorder strengths. The enhanced stability results from two special properties of 1D quasiperiodic Hamiltonians: first, Anderson localization [25] of the eigenstates even in the absence of additional disorder, and second, the bounded Cantor set spectrum of quasiperiodic operators – a closed no-where dense set for which any element itself is a limit point with a fractal hierarchy of gaps [26] – whose integrated density of states (IDoS) is quantized by the gap labeling theorem [27–29]. Further, we discuss how the robustness can be readily probed within existing cold atoms experiments, and leveraged to prepare many-body states with arbitrary Chern number.

While our results generalize to other short-range, bounded, analytic quasiperiodic Hamiltonians,¹ we focus on the prototypical Aubry-André-Harper (AAH) model as realized in e.g. optical lattices [30, 31], photonic systems [5], or with cavity polaritons [32] and known as the almost Mathieu operator in the mathematical physics lit-

* emg69@cam.ac.uk

† dborgnia@berkeley.edu

‡ rjs269@cam.ac.uk

§ uws20@cam.ac.uk

¹ Our results rest on the gap labeling theorem and Anderson localization which hold for this broad class of quasiperiodic models [25, 27].

erature

$$\hat{H}_{AAH}^{J,V}(\varphi) = \hat{V}(\varphi) - \hat{J}, \quad (1)$$

consisting only of a nearest-neighbor hopping term

$$\hat{J} = \sum_x J(\hat{a}_{x+1}^\dagger \hat{a}_x + \hat{a}_x^\dagger \hat{a}_{x+1}) \quad (2)$$

and an on-site cosine potential

$$\hat{V}(\varphi) = \sum_x 2V \cos(2\pi\beta x + \varphi) \hat{a}_x^\dagger \hat{a}_x, \quad (3)$$

where $x \in \mathbb{Z}$ denotes the lattice sites and a_x (a_x^\dagger) the corresponding annihilation (creation) operators for single particles. For irrational $\beta \in \mathbb{R} \setminus \mathbb{Q}$, $\hat{V}(\varphi)$ breaks the translation invariance of \hat{J} and the resulting eigenfunctions are Anderson localized for $|V/J| > 1$ [25] and extended for $|V/J| < 1$ [33], as a result of self-duality [34] around the critical point $V/J = 1$. We restrict $\beta \in (0, 1)$ without loss of generality and set $\beta = \sqrt{2}/2$ in all figures. Though pumping is then implemented by linearly increasing the phase φ in time at a constant pumping rate $\dot{\varphi} > 0$.

I. AAH: ENERGY GAPS AND CONFIGURATION SPACE

In periodic systems, the Brillouin zone offers a suitable base manifold on which to calculate topological invariants and band structures. To circumvent the lack of a Brillouin zone for quasiperiodic lattices, we construct a *configuration space* representation of the clean AAH chain, see Fig. 1 b. This representation offers a powerful language to discuss such quasiperiodic systems and enables a simple perturbative argument to derive the positions of the energy gaps, their labels, and exact expressions for their respective integrated densities of state. It is based on the observation that the only degree of freedom that differentiates one lattice site from another is the local value of the phase of the quasiperiodic modulation in Eq. (3). Therefore, labeling the sites with the local phase of the modulation offers a convenient description of the problem. In this configuration space representation, the position of site i is mapped to the angle θ_i on the unit circle according to

$$\theta_i = 2\pi\beta i + \varphi \pmod{2\pi}, \quad (4)$$

see Fig. 1b. Since β is irrational, this map is ergodic and the set of all possible θ_i , $\{\theta_i\}_{i \in \mathbb{Z}}$, densely and uniformly populates the unit circle, implying that every site is identified by a unique value of θ .

The Hamiltonian in Eq. (1) can then be re-expressed on the densely populated unit circle:

$$\hat{H}_{AAH}^{J,V} = 2V \sum_\theta \cos \theta \hat{a}_\theta^\dagger \hat{a}_\theta - J \sum_\theta (\hat{a}_\theta^\dagger \hat{a}_{\theta+2\pi\beta} + h.c.), \quad (5)$$

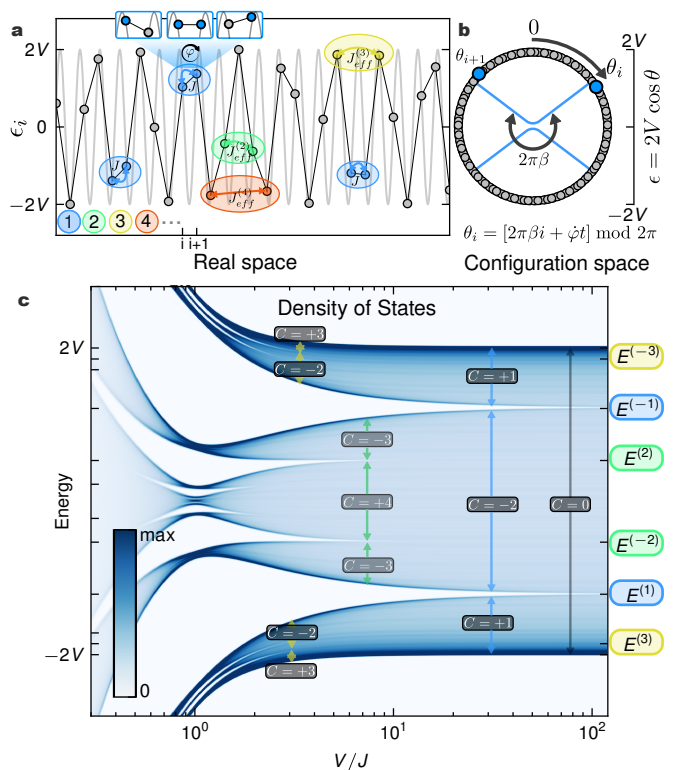


FIG. 1. **Perturbative derivation of the AAH energy spectrum:** (a) AAH chain where grey line denotes the quasiperiodic modulation of onsite energies ϵ_i , and circled dots are lattice sites. Solid lines indicate sites connected by the tunneling \hat{J} . Resonances between n -th nearest neighbors (blue ellipses show the $n = 1$ resonances) are mediated by an exponentially decreasing effective tunneling rate $J_{eff}^{(n)} \propto J^n/V^{n-1}$. (b) We map the AAH chain onto a uniformly dense unit circle – referred to as configuration space. In this representation, nearest-neighbors are separated by an angle $\theta_{i+1} - \theta_i = 2\pi\beta$, and the resonances occur at fixed angles $\theta^{(n)}$ (blue lines show $n = 1$ resonances). (c) The resonances result in a dense set of infinitely many pairs of energy gaps labelled by the integer n , which for $V \gg J$ lie at energies $E^{(\pm n)}$ (we show gaps up to $n = 3$, but all gaps are open for all values of V/J). Sets of states surrounded by two selected gaps acquire a Chern number fixed by the labels of the surrounding gaps (we show the Chern numbers of bands up to $n = 3$). Parameters: $\beta = \sqrt{2}/2$.

where \hat{a}_θ is the annihilation operator for a particle at coordinate θ in configuration space, and the second term reflects the fixed phase relation between real-space nearest-neighbors: $\theta_{i+1} - \theta_i = 2\pi\beta$. Importantly, sites that are close in configuration space can be arbitrarily far away in real space. However, due to the continuity of the cosine function, they will not only have similar energies but will also be surrounded by similar local configurations of lattice sites in real space.

In the absence of tunneling ($J/V = 0$), the spectrum

$$\sigma(\hat{H}_{AAH}) = \bigcup_{i \in \mathbb{Z}} (2V \cos(\theta_i)) \quad (6)$$

is dense on the interval $[-2V, 2V]$ (see right-hand side of Fig. 1 c), and every eigenstate is localized on a single lattice site. Turning on a small tunneling amplitude ($J/V \ll 1$), nearest neighbors whose onsite energy difference is small $\delta E = \epsilon_{i+1} - \epsilon_i \ll J$ (referred to as resonant neighbors, marked in blue in Fig. 1 a) hybridize and form (anti-) symmetric dimers, separated by the energy $\Delta E^{(1)} = 2J$. In addition, nearly resonant neighbors with similar onsite energies will also be affected by this hybridisation-induced level repulsion.

These resonances happen at fixed positions in configuration space, namely where neighboring sites at θ and $\theta + 2\pi\beta$ have similar onsite energies, i.e.,

$$\cos \theta^{(1)} \approx \cos(\theta^{(1)} + 2\pi\beta), \quad (7)$$

and the involved sites are connected by blue lines in Fig. 1 b. The resulting level repulsion opens a pair of spectral gaps of size $\Delta E^{(1)} \approx 2J$ at energies $\pm 2V \cos \pi\beta$ that split the spectrum into three *first-order bands* (indicated by blue arrows in Fig. 1 c). The IDoS of each of these bands is equal to the angle spanned by the band in configuration space. For instance, the lowest and highest first-order bands therefore contain, for $\beta > 1/2$, $(1 - \beta)$ states each, while the middle band contains $(2\beta - 1)$ states, where we normalise the total number of states to 1.

This perturbative analysis can directly be extended by looking for pairs of resonant sites at increasing distances $n > 1$. In n -th order, tunneling causes hybridisation of resonant n -th-nearest neighbors, mediated by an effective tunneling amplitude of order $J_{\text{eff}}^{(n)} \propto J^n/V^{n-1}$. The corresponding resonance conditions are:

$$\cos \theta^{(n)} \approx \cos(\theta^{(n)} + n 2\pi\beta), \quad (8)$$

which causes the opening of a pair of gaps of size $\Delta E^{(n)} \propto 2J^n/V^{n-1}$, at energies

$$E^{(\pm n)} = \begin{cases} \pm 2V \cos(n\pi\beta) & \text{if } [n\beta] \text{ even} \\ \mp 2V \cos(n\pi\beta) & \text{if } [n\beta] \text{ odd} \end{cases}. \quad (9)$$

Here, $[n\beta]$ refers to the integer part of $n\beta$. Eq. (9) shows that the AAH spectrum contains an infinite hierarchy of pairs of gaps – forming a dense set – labelled by the integer Chern numbers $\pm n$, where the two branches of the equation ensure consistency with the direction of quantized currents (see Appendix A for details). By the gap labelling theorem, every band, i.e., the set containing all states between two selected energy gaps, is indexed by a virtual Chern number [6] fixed by the difference between the two surrounding gap labels (Fig. 1 c). This Chern number is referred to as “virtual” in the sense that it is defined by treating φ as a virtual dimension of the system. It arises from the non-commutativity of x, ∂_φ -translations in configuration space analogous to the non-commutativity of x, y -translations responsible for the integer quantum hall effect [6, 35, 36].

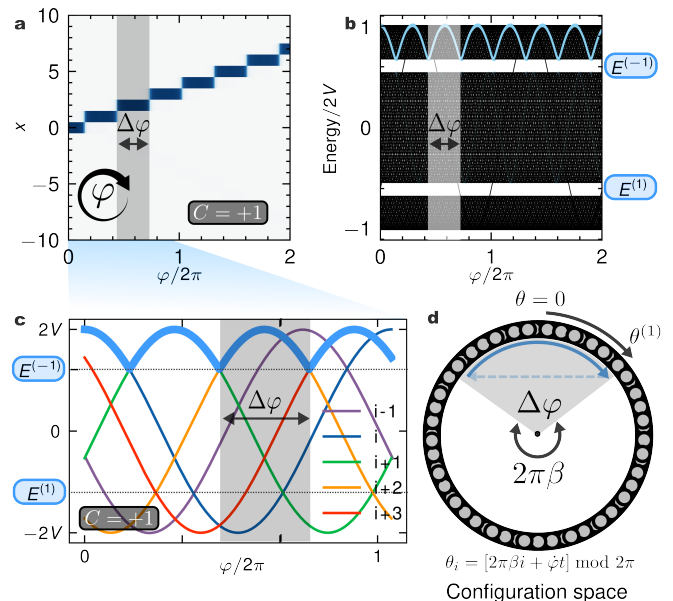


FIG. 2. **Thouless pumping in the clean AAH chain:** (a) Thouless pumping of a single strongly localized state in the upper $C = +1$ band, shown in real space. (b) Due to adiabaticity with respect to the first-order gaps, the state remains confined within its energy band. Blue curve shows the projection of the wavefunction onto the instantaneous eigenstates shown in black. (c) The Thouless pump can be understood by noting that the particle undergoes an adiabatic Landau-Zener (light blue curve in c) every time it crosses in energy with a resonant n -th neighbor (here we show $n = 1$). (d) In the configuration-space picture, pumping acts as a rotation (blue arrow); and particles in the top $C = +1$ band undergo one Landau-Zener transition (blue dashed arrow) for every $\Delta\varphi = 2\pi(1 - \beta)$. The same argument can be extended to any of the energy bands. Parameters: $\beta = \sqrt{2}/2$. $J = 1$, $V = 7.5$, $W/(2V) = 0$. $\dot{\varphi} = 5 \cdot 10^{-2}$.

While the above gap construction relies on the hierarchy of effective tunnelings $J_{\text{eff}}^{(n+1)} \ll J_{\text{eff}}^{(n)}$ to generate a hierarchy of spectral gaps, as mentioned above, the spectrum indeed forms a no-where dense Cantor set and the IDoS is constant for all $V/J \neq 1$ [26, 28], extending the results of the above analysis to any value of $V/J > 1$ and by self-duality to $V/J < 1$.

II. THOULESS PUMPING IN THE AAH MODEL

Thouless pumping is a special case of adiabatic transport that occurs under a continuous, slow, and periodic modulation of the Hamiltonian. If the path in parameter space encloses a non-trivial topological charge, and the modulation is slow enough to not induce excitations out of the occupied subspace, the pumping gives rise to a quantized current proportional to the value of this charge [3].

The Hamiltonian $\hat{H}_{\text{AAH}}^{J,V}(\varphi)$ is smooth and periodic in

φ and, as discussed before, its spectrum forms a Cantor set independent of φ whose gaps are labeled by Chern numbers [26]. Since a Cantor set is nowhere dense, the spectrum is separated into arbitrarily many “bands”

$$B^{(m,n)} \subset \sigma \left(\hat{H}_{AAH}^{J,V}(\varphi) \right), \quad (10)$$

isolated by spectral gaps $\Delta E^{(m)}, \Delta E^{(n)}$ at energies $E^{(m)}, E^{(n)}$ independent of $\varphi \in [0, 2\pi)$. This guarantees the existence of smooth contours $\gamma_{m,n}(\varphi)$ in the complex energy plane containing all of $B^{(m,n)}$ for all φ , which in turn guarantees adiabatic transport in the $\dot{\varphi} \rightarrow 0$ limit [37]. Thus, the 1D system evolving under $\hat{H}_{AAH}^{J,V}(\varphi(t))$ with $\varphi(t) = 2\pi\dot{\varphi}t + \varphi_0$ and $(\hbar 2V\dot{\varphi})^{1/2} \ll \min(\Delta E^{(m)}, \Delta E^{(n)})$ constitutes a Thouless pump and results in a quantized current proportional to the band’s Chern number. The current

$$\hat{I}(t) = \frac{i}{L} J \sum_{x=1}^L (\hat{a}_{x+1}^\dagger \hat{a}_x - \hat{a}_x^\dagger \hat{a}_{x+1}) \quad (11)$$

is the spatial average of the current operator over the system (of length L), and is computed as the derivative of the total pumped charge $I \equiv \partial_\varphi Q$ averaged over the entire system. In contrast to periodic systems, where the current is time-dependent and only the pumped charge per pump cycle is quantized, the current itself is time independent and quantized in the quasiperiodic case [12], by the invariance of the spectrum with respect to φ .

For a given pump rate $\dot{\varphi}$, the Cantor set spectrum consists of finitely many larger (adiabatic) gaps with $(\Delta E)^2 \gg \hbar 2V\dot{\varphi}$ that are traversed adiabatically during the pumping, and infinitely many smaller (diabatic) gaps with $(\Delta E)^2 \ll \hbar 2V\dot{\varphi}$ that are irrelevant for the pumping dynamics. Hence only the adiabatic gaps need be considered. For decreasing pump rates, more and more gaps become adiabatic and the effective bands split into new bands indexed by typically larger Chern numbers. For instance, once the 2nd-order gaps become adiabatic, the central $C = -2$ 1st-order band splits into three bands with $C = -3, +4, -3$, which together add up to $C = -2$ (see Fig. 1 c).

The above division into adiabatic and diabatic gaps is particularly powerful in the regime $V/J \gg 1$, where the separation in energy gaps $\Delta E^{(n)}/\Delta E^{(n+1)}$ is largest. Moreover, in this regime, Anderson localization permits an effective model (with exponential precision in V/J) in which eigenstates are completely localized on a single site. In this regime, the configuration space representation offers a local, geometric view of adiabatic pumping, see Fig. 2: an increase in φ acts as a clockwise rotation in configuration space (Fig. 2 c and d) and by continuously varying φ , every single-site localized state eventually reaches a resonance, $\theta^{(n)}$, where it resonates with another state localized n sites away. The dynamics of the two resonant sites is well approximated by an effective 2-

by-2 Hamiltonian

$$H_{2 \times 2}^{(n)}(t) = \begin{pmatrix} \delta^{(n)}(t)/2 & J_{eff}^{(n)} \\ J_{eff}^{(n)} & -\delta^{(n)}(t)/2 \end{pmatrix} \quad (12)$$

whose detuning

$$\delta^{(n)}(t) = 2V \left[\cos \left(\theta^{(n)} + \varphi(t) \right) - \cos \left(\theta^{(n)} + 2n\pi\beta + \varphi(t) \right) \right] \quad (13)$$

varies continuously, with one site going up in energy while the other goes down with φ , see inset Fig. 1a. If the gap is adiabatic ($(\Delta E)^2 \gg \hbar 2V\dot{\varphi}$), i.e., the pump rate $\dot{\varphi}$ is slow compared to the corresponding tunneling process $J_{eff}^{(n)} \propto J^n/V^{n-1}$, the state adiabatically follows an eigenstate of the Rabi Hamiltonian and undergoes a Landau-Zener transition to the resonant n -th order neighbor – giving rise to the quantized transport. In configuration space, this Landau-Zener tunnelling translates into a discrete jump of $2\pi\beta n$.

The quantized current for a given filled band (in the case $\beta > 1/2$) can be inferred as follows: In the upper first-order band, indicated by the shaded sector in Fig. 2 d, states are rotated along the blue arrow and will on average undergo a Landau-Zener transitions every time the phase winds by $\Delta\varphi = 2\pi(1 - \beta)$. Since in this band the transition is to the neighboring site ($n = 1$), every state is transported by on average $1/(1 - \beta)$ sites per pump cycle. Combined with the fraction $(1 - \beta)$ of states in the this band, the total pumped charge per pump cycle in this band is $C_p = (1 - \beta) \frac{1}{1 - \beta} = +1$, from which we extract $C = +1$. The cases where $\beta < 1/2$ can be treated by sending $\beta \rightarrow 1 - \beta$.

The Chern number of any given band can similarly be extracted from this local picture by computing the total current over one cycle for all states in some filled band $B^{(m,n)}$ containing only diabatically small gaps enclosed between two adiabatically large spectral gaps $\Delta E_m, \Delta E_n$.

The configuration-space picture matches an alternative, global computation of the quantized current using the smooth projector

$$\hat{P}^{(m,n)}(\varphi) = \oint_{\gamma_{m,n}(\varphi)} dz \left(z - \hat{H}_{AAH}^{J,V}(\varphi) \right)^{-1}, \quad (14)$$

see Ref. [37] for further details. In the absence of disorder (see below), the adiabatic transport resulting from both the projector and the local Landau-Zener picture are equivalent by Theorem 1.2 in Ref. [38]. However, the proof of quantized currents in the projector picture depends on a global condition, namely the existence of sufficiently large spectral gaps in the spectrum of $\hat{H}_{AAH}^{J,V}(\varphi)$. By contrast, the Landau-Zener transitions in the configuration-space picture depend only on local resonance conditions. This key difference allows the configuration-space picture to be extended to strong disorder.

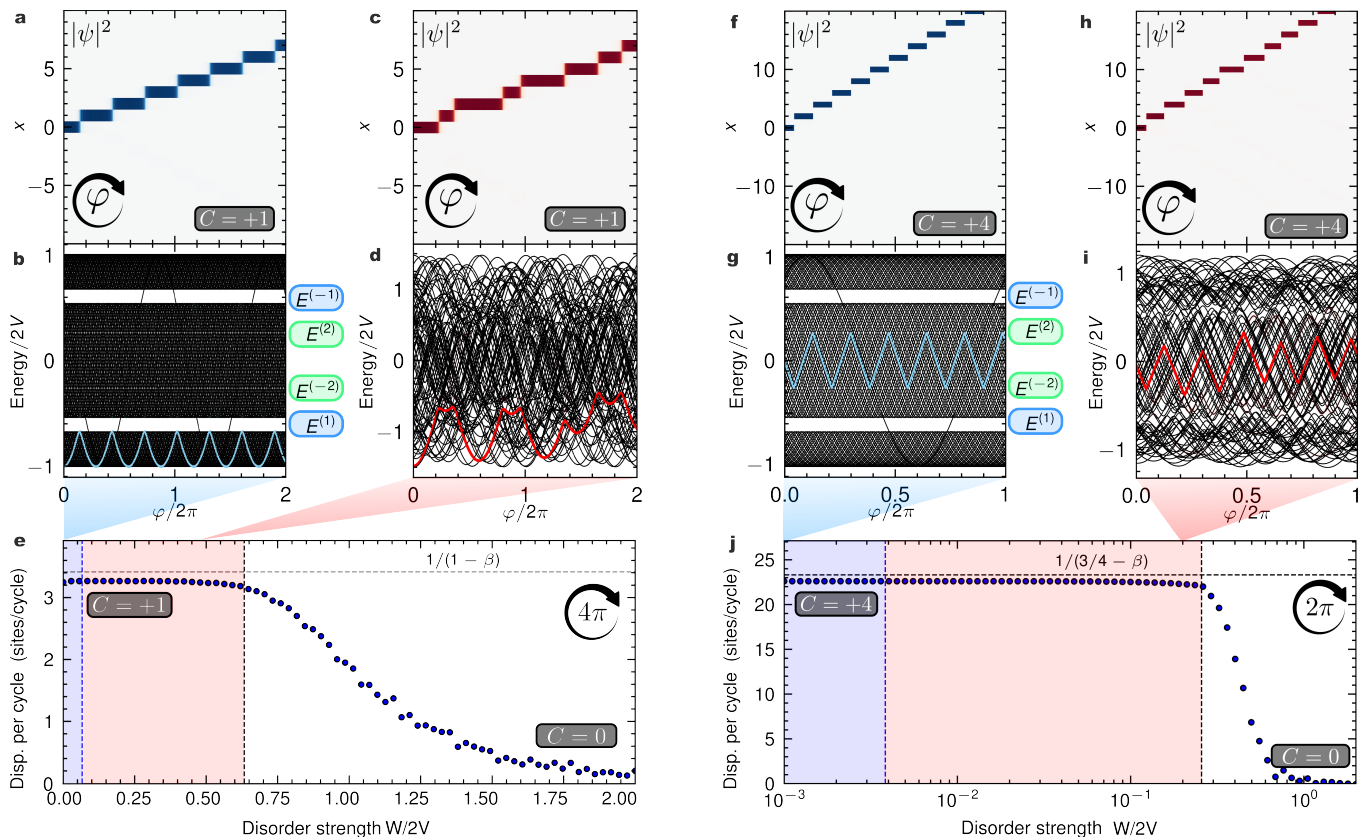


FIG. 3. **Stability and breakdown of quantized currents under on-site disorder:** Left side shows results for the lower $C = +1$ first-order band, while the right side concerns the $C = +4$ second-order band. (a,f) Thouless pumping of a particle in the clean case $W = 0$, resulting in a quantized average displacement per cycle. (b,g) the particle stays confined within its energy band surrounded by open gaps throughout the Thouless pump (blue curve shows the projection of the wavefunction onto the instantaneous eigenstates in black). (c,h) In the disordered case, the averaged displacement remains quantized, despite the energy gaps being closed (d,i) by the disorder. (e,j) Average displacement per pump cycle after 2 (e) or 1 (j) pump periods, showing quantisation also past the closing of the clean energy gaps (red region). The observed critical disorder strengths are in excellent agreement with our proposed geometric argument (Eq. (B5), Eq. (C4), vertical black dotted lines), and for $C = +4$ is more than an order of magnitude larger than the gaps. Horizontal dotted lines indicate the current expected in the clean limit for an infinite pump period. Each point is obtained after averaging over 1000 disorder realisations. Parameters: $\beta = \sqrt{2}/2$, $J = 1$, $V = 7.5$, $\dot{\varphi} = 5 \cdot 10^{-2}$ for $C = +1$, and $\dot{\varphi} = 10^{-4}$ for $C = +4$.

III. ROBUSTNESS TO SPATIAL DISORDER

We will now add local disorder

$$\hat{W} = \sum_n w_n \hat{a}_n^\dagger \hat{a}_n, \quad (15)$$

where the $w_n \in [-W, W]$ are independent, identically distributed random variables. The full disordered Hamiltonian is then

$$\hat{H}^{J,V,W}(\varphi) = \hat{H}_{AAH}^{J,V}(\varphi) + \hat{W}. \quad (16)$$

Its eigenfunctions are all Anderson localized both by the disorder \hat{W} [39] and, for $V > J$, by the famous Aubry-André duality mentioned above [25].

It was shown in [40] that the resulting spectrum $\sigma(\hat{H}^{J,V,W}(\varphi))$ is the span of the pairwise sum of elements in the unperturbed spectrum $\sigma(\hat{H}_{AAH}^{J,V}(\varphi))$ with

elements from the disorder distribution $[-W, W]$,

$$\sigma(\hat{H}^{J,V,W}(\varphi)) = \sigma(\hat{W}) \star \sigma(\hat{H}_{AAH}^{J,V}(\varphi)). \quad (17)$$

Intuitively, this means that the disordered energy spectrum can be obtained by convolving the clean spectrum with the spectrum of the disorder term. Therefore, it follows that the disorder closes all unperturbed spectral gaps that are smaller than the bandwidth of the disorder strength $\Delta E^{(n)} < 2W$.

We numerically compute the pumped charge as the average number of sites traveled per pump cycle from a linear fit of the center of mass motion for a single particle initially localized in a band with Chern number $C = +1$ (Fig. 3 a) and $+4$ (Fig. 3 f). For small disorders (blue shaded area), the extracted values agree as expected with the above quantized predictions in the presence of global gaps, see Fig. 3 e, j. However, the quantized currents

survive far beyond the closing of the clean energy gaps (dashed blue lines), and break down only at larger critical disorder strengths (dashed black vertical lines). In the $C = +4$ band shown in Fig. 3 j, we find that the critical disorder strength for this particular band exceeds the size of the clean $\Delta E^{(\pm 2)}$ gaps by more than an order of magnitude. These critical disorder strengths are band-dependent even if the bands share a gap, see Appendix B.

Once more, configuration space provides a simple local picture for the stability of the quantized current as well as the band-dependent critical disorder strength. In the clean case, the phase winding $\Delta\varphi$ between two consecutive Landau-Zener processes for a given localized state is constant (Fig. 4 a,b) and corresponds to the angle spanned by the corresponding resonance on the unit circle, see Fig. 2d. In the presence of disorder, this phase fluctuates randomly, giving rise to a distribution of spatially-dependent and randomly distributed $\Delta\varphi_i = \Delta\varphi + \delta\varphi_i$. This is reflected in the fluctuating size of the plateaus in Fig. 3 c. As long as the disorder is below a critical value (which we calculate in Appendix B), these fluctuations $\delta\varphi_i$ average to zero and leave the quantized current unaffected (Fig. 4 c,d). Once the disorder becomes strong enough to shrink one or more of the $\Delta\varphi_i$ down to 0 (Fig. 4 e,f), the order of resonances may change, which results in the breakdown of the quantized current as the particle starts being back-reflected.

Thus, the robustness of the quantized current is not limited by the size of the clean energy gaps, but instead depends on the ordering of consecutive local resonances. In the clean case, these resonances are all aligned in energy, giving rise to a global gap. Increasing onsite disorder shifts each resonance independently and thereby closes the global energy gaps, but does not necessarily modify their ordering. As long as the order between consecutive local resonances remains unaffected, quantized currents can subsist, even in the complete absence of global energy gaps in the system. Notably, bands for which $\Delta\varphi$ is larger, i.e., those which have a larger IDoS, are more robust to fluctuations $\delta\varphi_i$. This constitutes a novel form of topological protection.

IV. EXPERIMENTAL SIGNATURES AND QUANTUM STATE PREPARATION

The robustness of the quantized currents can not only be directly observed experimentally, but can also be leveraged to turn the Thouless pump into a robust protocol for preparing quantum states with desired Chern numbers. We propose here an instance of the protocol that is directly implementable within existing cold atom experiments.

The one-dimensional AAH model can be realised by superimposing one strong (primary) optical lattice with another weaker incommensurate lattice [12, 23, 30, 31], where deep lattices in the transverse directions confine

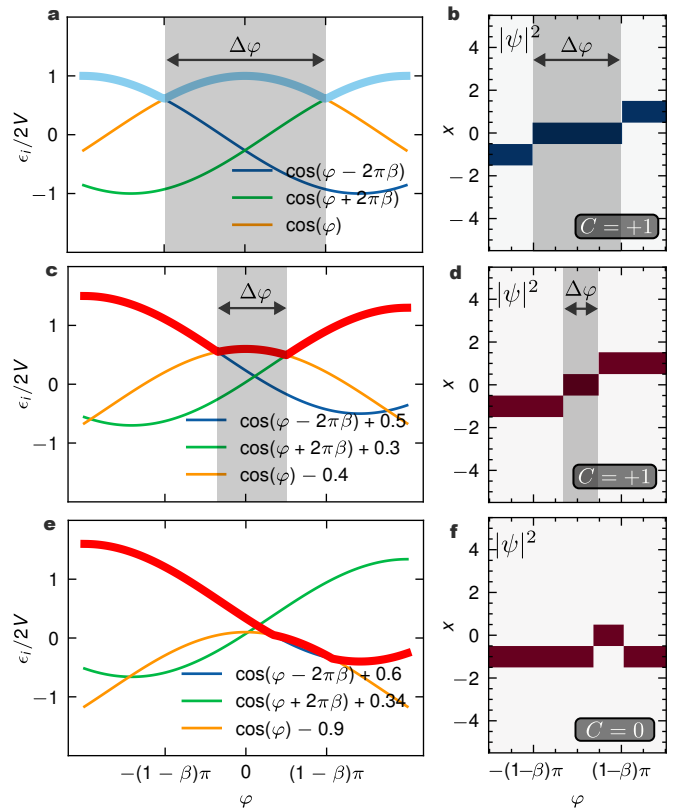


FIG. 4. **Local argument for the stability and breakdown of quantized currents:** Coloured lines in the left column panels are on-site energies of consecutive neighbors. Thick coloured line illustrates the adiabatic trajectory of the state under pumping for $V \gg J$, whose real-space density is shown in the right column. (a,b) In the clean case, the phase $\Delta\varphi$ separating two consecutive Landau-Zener transitions is constant, and the particle undergoes successive adiabatic transitions to neighboring sites at a constant rate (blue curve). (c,d) The addition of not-too-large onsite disorder induces fluctuations in the phase $\Delta\varphi$ between transitions, but leaves the pumped current quantized. (e,f) When the disorder strength exceeds a critical value, the order of successive Landau-Zener processes can be changed, causing the particle to be backreflected. The argument is shown here for the top $C = +1$ first-order band, but can be easily applied to any other band. Parameters: $\beta = \sqrt{2}/2$.

the atoms to 1D chains. The depth of the primary lattice sets J and the depth of the secondary lattice depth provides control over V/J . The same model can also be realized by independently controlling the depths of the individual lattices in an optical quasicrystal [41–43]. For large systems, the initial phase φ of the quasiperiodic modulation is irrelevant. The initial state can be prepared for instance as a unit-filling band insulator of spinless fermions or hard-core bosons in a projected optical box potential [44]. Such a state naturally samples the energy spectrum uniformly.

In contrast to periodic systems, the AAH system can be realised in the regime $V \gg J$, where all eigenstates

are strongly localized. In this regime, the only motion stems from the pumping, and the atomic cloud will not undergo any free expansion, such that no additional trap is required.

States in different bands become spatially separated as φ is pumped. For example, if the pumping rate is set to be adiabatic with respect to the first-order gaps only, the Thouless pump splits the cloud in two parts (Fig. 5). The right moving part corresponds to atoms populating the lower and upper bands with $C = +1$, while the left-moving part contains the atoms in the middle band with $C = -2$. Note that the center of mass position of the entire cloud remains constant at all times, since the total Chern number of the entire spectrum vanishes ($C = 0$). To prepare a state with the desired Chern number, it then suffices to select the desired branch by clearing out atoms in the (spatially separated) undesired branches by, for example, exposing them to resonant laser light.

The Thouless pump can be made sensitive to increasingly smaller gaps, and hence higher Chern numbers, by reducing the pumping rate $\dot{\varphi}$, leading to successive branchings of the final density, see Fig. 6. The robustness of the Thouless pump to onsite disorder ensures that this state preparation protocol is robust even when the energy gaps surrounding the targeted energy bands are small. This protocol can be directly extended to the interacting regime by using fermionic spin mixtures or real bosons and tuning the onsite interaction strength via a Feshbach resonance [45].

The above procedure generates a 1D many-body state with an associated virtual Chern number. To generate a state with a well-defined “real” 2D Chern number, the protocol can in principle be extended to a 2D lattice consisting of an array of n_y AAH chains with increasing phase $\varphi(y) = 2\pi y/n_y$ along a second spatial dimension y . This results in a 2D Hamiltonian given by

$$\hat{H}_{2D} = \sum_{(x,y)} 2V \cos\left(2\pi\beta x + \frac{2\pi}{n_y}y\right) \hat{a}_{x,y}^\dagger \hat{a}_{x,y} - J \left(\hat{a}_{x+1,y}^\dagger \hat{a}_{x,y} + \hat{a}_{x,y}^\dagger \hat{a}_{x+1,y} \right), \quad (18)$$

whose spectrum is the same as that of the 1D AAH Hamiltonian [34, 46]. Under Fourier transforming $y \rightarrow \tilde{y}$, Eq. (18) is equivalent to the 2D Harper Hamiltonian

$$\hat{H}_{QHE} = \sum_{(x,\tilde{y})} V \left(e^{i2\pi\beta x} \hat{a}_{x,\tilde{y}+1}^\dagger \hat{a}_{x,\tilde{y}} + h.c. \right) - J \left(\hat{a}_{x+1,\tilde{y}}^\dagger \hat{a}_{x,\tilde{y}} + h.c. \right), \quad (19)$$

which describes a square lattice with magnetic flux $2\pi\beta$ per plaquette. Therefore, by stacking multiple copies of the one-dimensional state preparation protocol, we prepare a state with a desired Chern number of the 2D Harper Hamiltonian, albeit in a mixed real-momentum space configuration. The chains can be coupled by introducing small tunneling terms between neighboring chains

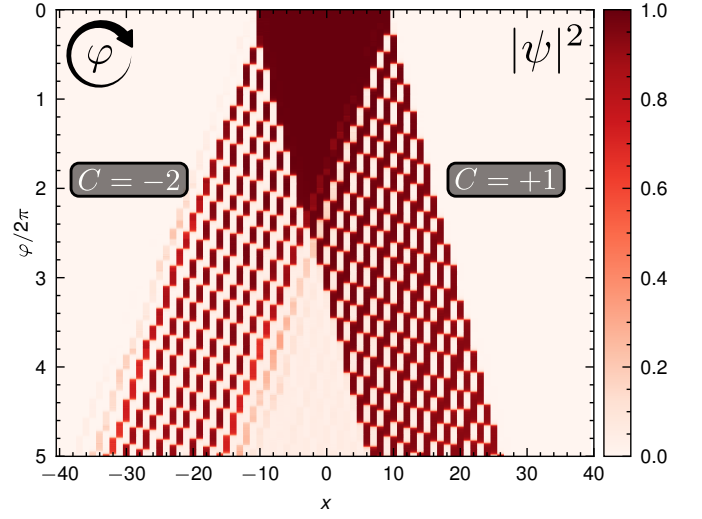


FIG. 5. Preparing states with desired Chern numbers: The initial state is prepared as a product of local Fock states with unit filling and the pumping rate $\dot{\varphi}$ is chosen to be adiabatic with respect to the first-order gaps only. The atom cloud splits into a left- and a right-moving part that move at different speeds, separating the middle band with Chern number $C = -2$ from the top and bottom bands with $C = +1$. The desired Chern number can be selected by e.g. eliminating the remaining other branches with a resonant laser pulse. *Parameters:* $\beta = \sqrt{2}/2$, $J = 1$, $V = 7.5$, $W/(2V) = 0.3$. $\dot{\varphi} = 5 \cdot 10^{-2}$.

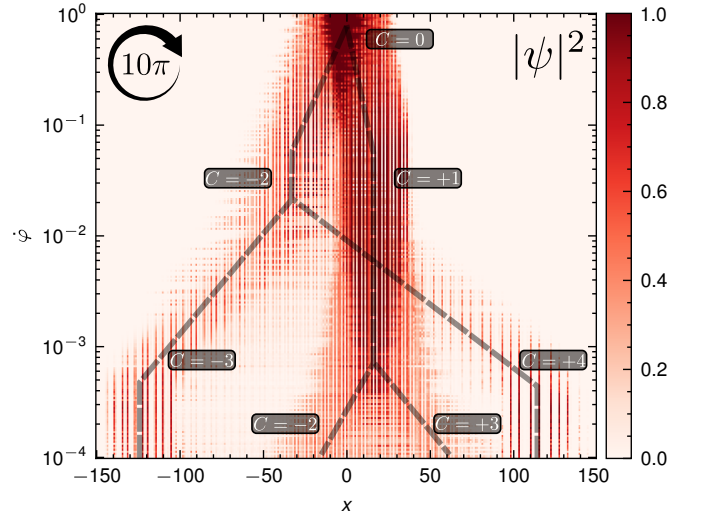


FIG. 6. Effect of pumping rate: Final density after 5 pump cycles for various pump rates $\dot{\varphi}$. The initial state is a Fock state with one atom per site within a selected region. By decreasing the pump rate $\dot{\varphi}$, the Thouless pump becomes sensitive to smaller gaps, characterised by increasingly higher Chern numbers. This is reflected in the successive branchings of the final density as the pumping rate is decreased, highlighted by the dashed guidelines. *Parameters:* $\beta = \sqrt{2}/2$, $J = 1$, $V = 5$, $W/(2V) = 0.01$.

without altering the Chern number of the state, provided that the spectral gaps remain open [47].

Interestingly, on-site interactions effectively appear as local momentum-space interactions in the y coordinate [48]. This mixed real-momentum space system presents an opportunity to probe new quantum Hall physics inaccessible to traditional condensed-matter systems, e.g. one could engineer local scalar potentials in momentum space to reproduce dispersion relations corresponding to long-range real-space hopping models which have been used to generate exact fractional quantum hall (FQH) phases on a lattice via topological flat bands [49], and non-local real-space interactions have been used to stabilize non-abelian fractional Chern insulator (FCI) phases in numerics [50]. Moreover, numerical studies of fractional Chern insulators have long noticed enhanced stability of the FCI phase in higher Chern number bands [51] along with new phases of matter with no FQH analogs [52]. As such, the above state preparation protocol could become a new experimental platform for exploring numerous theoretical proposals involving large Chern numbers, flat bands, and non-local interactions.

V. DISCUSSION AND CONCLUSION

We present a novel example of topological protection in quasiperiodic systems depending on the number of states and the position of the band in configuration space rather than a spectral gap condition, challenging the traditional understanding that the robustness of topological phenomena depends on the presence of spectral gaps [37], mobility gaps [17], or symmetry protections [19]. By tracking the fate of quantized currents in the disordered Aubry-André chain (1D almost Mathieu operator), we find that the combination of quasiperiodic Anderson localization and the gap labelling theorem results in a robustness to bounded local disorder far beyond the closing of the relevant spectral gaps. We furthermore develop a local picture to explain quasiperiodic Thouless pumping both in the clean and disordered case that provides excellent estimates for the numerically observed critical disorder strengths.

The outlined mathematical relations to ergodicity and the Dry Ten Martini problem [26, 28, 29] ensure pathways to generalizations. In one-dimension, it would be worth exploring the case of several incommensurate frequencies, which are likely to result in enhanced stabilization mechanisms that in turn should lead to novel measurable signatures. These pursuits can also be followed in the context of the Dry Ten Martini problem without dualities or with hidden dualities [28, 29, 53], where localization phase transitions may be richer.

In two-dimensional systems, the presence of second Chern numbers and a richer set of topological invariants could lead to more examples of gap-independent topological protection. For example, in ultracold atomic systems, the scheme could be extended to the two-

dimensional Aubry-André model or optical quasicrystals [41–43], where pumping could be realised along multiple dimensions. The recent advent of moiré van der Waals structures, in which pumping can be achieved upon applying periodic external gauge fields, provides for an exciting solid-state platform in which these new mechanisms might both occur and help explain experimental observations.

In summary, our results uncover a novel protection mechanism for Thouless pumping, highlighting an unexplored richness of topology in quasiperiodic systems and motivating a re-examination of topological protection in the absence of translation invariance. They furthermore enable novel experimental applications, notably in the preparation of quantum states with high Chern numbers.

VI. ACKNOWLEDGEMENTS

We cordially thank Joel E. Moore for insightful feedback and advice regarding the draft. We also thank Arjun Ashoka, Alexander Avdoshkin, Vir B. Bulchandani, Fabian Heidrich-Meisner, Matthew Henricks, Johannes Mitscherling, Suman Mondal, Lee Reeve, Ruben Verresen, Qijun Wu, and Maciej Zworski for many helpful discussions. R.-J.S. acknowledges funding from a New Investigator Award, EPSRC grant EP/W00187X/1, a EPSRC ERC underwrite grant EP/X025829/1, and a Royal Society exchange grant IES/R1/221060 as well as Trinity College, Cambridge. Work by D.S.B. was performed with support through a MURI project supported by the Air Force Office of Scientific Research (AFSOR) under grant number FA9550-22-1-027. U.S. and E.G. acknowledges support by the European Commission ERC Starting Grant QUASICRYSTAL, the EPSRC Grant (No. EP/R044627/1), and EPSRC Programme Grant DesOEQ (No. EP/P009565/1). E.G. acknowledges support from the Cambridge Trust. For the purpose of open access, the authors have applied a Creative Commons Attribution (CC BY) licence to any Author Accepted Manuscript version arising from this submission.

VII. AUTHORS CONTRIBUTIONS

E. G. with input from U. S. set up and performed the numerical and analytical configuration-space analysis for the Thouless pump. Relations to mathematical spectral theory and the discovery of the underlying stability mechanism under disorder progressed with insights from D. S. B. and R.-J. S.. D. S. B. had a steering role in turning to the stability under disorder. All aspects were extensively discussed amongst all authors. All authors contributed to the writing of the manuscript.

-
- [1] D. J. Thouless, M. Kohmoto, M. P. Nightingale, and M. den Nijs, Quantized hall conductance in a two-dimensional periodic potential, *Physical Review Letters* **49**, 405 (1982).
- [2] B. I. Halperin, Quantized hall conductance, current-carrying edge states, and the existence of extended states in a two-dimensional disordered potential, *Physical Review B* **25**, 2185 (1982).
- [3] D. J. Thouless, Quantization of particle transport, *Physical Review B* **27**, 6083 (1983).
- [4] R. Citro and M. Aidelsburger, Thouless pumping and topology, *Nature Reviews Physics* **5**, 87 (2023).
- [5] Y. E. Kraus, Y. Lahini, Z. Ringel, M. Verbin, and O. Zilberberg, Topological states and adiabatic pumping in quasicrystals, *Physical Review Letters* **109**, 106402 (2012).
- [6] E. Prodan, Virtual topological insulators with real quantized physics, *Physical Review B* **91**, 245104 (2015).
- [7] T. Ozawa, H. M. Price, A. Amo, N. Goldman, M. Hafezi, L. Lu, M. C. Rechtsman, D. Schuster, J. Simon, O. Zilberberg, and I. Carusotto, Topological photonics, *Rev. Mod. Phys.* **91**, 015006 (2019).
- [8] M. Lohse, C. Schweizer, O. Zilberberg, M. Aidelsburger, and I. Bloch, A Thouless quantum pump with ultracold bosonic atoms in an optical superlattice, *Nature Physics* **12**, 350 (2016).
- [9] S. Nakajima, T. Tomita, S. Taie, T. Ichinose, H. Ozawa, L. Wang, M. Troyer, and Y. Takahashi, Topological Thouless pumping of ultracold fermions, *Nature Physics* **12**, 296 (2016).
- [10] A.-S. Walter, Z. Zhu, M. Gächter, J. Minguzzi, S. Roschinski, K. Sandholzer, K. Viebahn, and T. Esslinger, Quantization and its breakdown in a hubbard–thouless pump, *Nature Physics* **19**, 1471–1475 (2023).
- [11] K. Viebahn, A.-S. Walter, E. Bertok, Z. Zhu, M. Gächter, A. A. Aligia, F. Heidrich-Meisner, and T. Esslinger, Interactions enable thouless pumping in a nonsliding lattice, *Phys. Rev. X* **14**, 021049 (2024).
- [12] P. Marra and M. Nitta, Topologically quantized current in quasiperiodic Thouless pumps, *Physical Review Research* **2**, 042035 (2020).
- [13] A. Grabarits, A. Takács, I. C. Fulga, and J. K. Asbóth, Floquet-anderson localization in the thouless pump and how to avoid it, *Phys. Rev. B* **109**, L180202 (2024).
- [14] D. Vuina, D. M. Long, P. J. D. Crowley, and A. Chandran, Absence of disordered thouless pumps at finite frequency (2024), [arXiv:2401.17395 \[cond-mat.dis-nn\]](https://arxiv.org/abs/2401.17395).
- [15] J. E. Avron and A. Elgart, Adiabatic theorem without a gap condition, *Communications in mathematical physics* **203**, 445 (1999).
- [16] J. Avron, M. Fraas, G. Graf, and P. Grech, Adiabatic theorems for generators of contracting evolutions, *Communications in mathematical physics* **314**, 163 (2012).
- [17] R. B. Laughlin, Quantized hall conductivity in two dimensions, *Physical Review B* **23**, 5632 (1981).
- [18] A. Kitaev, Periodic table for topological insulators and superconductors, *AIP Conference Proceedings* **1134**, 22 (2009), https://pubs.aip.org/aip/acp/article-pdf/1134/1/22/11584243/22_1_online.pdf.
- [19] T. Scaffidi, D. E. Parker, and R. Vasseur, Gapless symmetry-protected topological order, *Physical Review X* **7**, 041048 (2017).
- [20] J. Kruthoff, J. de Boer, J. van Wezel, C. L. Kane, and R.-J. Slager, Topological classification of crystalline insulators through band structure combinatorics, *Physical Review X* **7**, 041069 (2017).
- [21] R. Verresen, R. Thorngren, N. G. Jones, and F. Pollmann, Gapless topological phases and symmetry-enriched quantum criticality, *Physical Review X* **11**, 041059 (2021).
- [22] M. M. Wauters, A. Russomanno, R. Citro, G. E. Santoro, and L. Privitera, Localization, topology, and quantized transport in disordered floquet systems, *Physical Review Letters* **123**, 266601 (2019).
- [23] S. Nakajima, N. Takei, K. Sakuma, Y. Kuno, P. Marra, and Y. Takahashi, Competition and interplay between topology and quasi-periodic disorder in Thouless pumping of ultracold atoms, *Nature Physics* **17**, 844 (2021).
- [24] A. L. C. Hayward, E. Bertok, U. Schneider, and F. Heidrich-Meisner, Effect of disorder on topological charge pumping in the Rice-Mele model, *Physical Review A* **103**, 043310 (2021).
- [25] S. Y. Jitomirskaya and Y. Last, Anderson localization for the almost mathieu equation, iii. semi-uniform localization, continuity of gaps, and measure of the spectrum, *Communications in mathematical physics* **195**, 1 (1998).
- [26] A. Avila and S. Jitomirskaya, The ten martini problem, *Annals of mathematics* , 303 (2009).
- [27] J. Bellissard, A. Bovier, and G. Jean-Michel, Gap labelling theorems for one dimensional discrete schrödinger operators, *Reviews in Mathematical Physics* **04**, 1 (1992).
- [28] A. Avila, J. You, and Q. Zhou, *Dry ten martini problem in the non-critical case* (2023).
- [29] R. Han, Dry ten martini problem for the non-self-dual extended harper’s model, *Transactions of the American Mathematical Society* **370**, 197 (2018).
- [30] G. Roati, C. D’Errico, L. Fallani, M. Fattori, C. Fort, M. Zaccanti, G. Modugno, M. Modugno, and M. Inguscio, Anderson localization of a non-interacting bose–einstein condensate, *Nature* **453**, 895–898 (2008).
- [31] M. Schreiber, S. S. Hodgman, P. Bordia, H. P. Lüschen, M. H. Fischer, R. Vosk, E. Altman, U. Schneider, and I. Bloch, Observation of many-body localization of interacting fermions in a quasirandom optical lattice, *Science* **349**, 842 (2015).
- [32] V. Goblot, A. Štrkalj, N. Pernet, J. L. Lado, C. Dorow, A. Lemaître, L. Le Gratiet, A. Harouri, I. Sagnes, S. Ravets, A. Amo, J. Bloch, and O. Zilberberg, Emergence of criticality through a cascade of delocalization transitions in quasiperiodic chains, *Nature Physics* **16**, 832–836 (2020).
- [33] S. Y. Jitomirskaya, Metal-insulator transition for the almost mathieu operator, *Annals of Mathematics* , 1159 (1999).
- [34] S. Aubry and G. André, Analyticity breaking and anderson localization in incommensurate lattices, *Ann. Israel Phys. Soc* **3**, 133 (1980).
- [35] D. S. Borgnia, A. Vishwanath, and R.-J. Slager, Rational approximations of quasiperiodicity via projected green’s functions, *Physical Review B* **106**, 054204 (2022).

- [36] D. S. Borgnia and R.-J. Slager, Localization as a consequence of quasiperiodic bulk-bulk correspondence, *Physical Review B* **107**, 085111 (2023).
- [37] T. Kato, On the adiabatic theorem of quantum mechanics, *Journal of the Physical Society of Japan* **5**, 435 (1950).
- [38] G. A. Hagedorn, Proof of the Landau-Zener formula in an adiabatic limit with small eigenvalue gaps, *Communications in Mathematical Physics* **136**, 433 (1991).
- [39] P. W. Anderson, Absence of diffusion in certain random lattices, *Physical Review* **109**, 1492 (1958).
- [40] A. Avila, D. Damanik, and A. Gorodetski, *The spectrum of Schrödinger operators with randomly perturbed ergodic potentials* (2022).
- [41] E. Gottlob and U. Schneider, Hubbard models for quasicrystalline potentials, *Physical Review B* **107**, 144202 (2023).
- [42] M. Sbroscia, K. Viebahn, E. Carter, J.-C. Yu, A. Gaunt, and U. Schneider, Observing localization in a 2d quasicrystalline optical lattice, *Physical Review Letters* **125**, 200604 (2020).
- [43] K. Viebahn, M. Sbroscia, E. Carter, J.-C. Yu, and U. Schneider, Matter-wave diffraction from a quasicrystalline optical lattice, *Physical Review Letters* **122**, 110404 (2019).
- [44] N. Navon, R. P. Smith, and Z. Hadzibabic, Quantum gases in optical boxes, *Nature Physics* **17**, 1334–1341 (2021).
- [45] C. Chin, R. Grimm, P. Julienne, and E. Tiesinga, Feshbach resonances in ultracold gases, *Rev. Mod. Phys.* **82**, 1225 (2010).
- [46] D. R. Hofstadter, Energy levels and wave functions of Bloch electrons in rational and irrational magnetic fields, *Phys. Rev. B* **14**, 2239 (1976).
- [47] S. Ryu, A. P. Schnyder, A. Furusaki, and A. W. Ludwig, Topological insulators and superconductors: tenfold way and dimensional hierarchy, *New Journal of Physics* **12**, 065010 (2010).
- [48] F. A. An, E. J. Meier, J. Ang'ong'a, and B. Gadway, Correlated dynamics in a synthetic lattice of momentum states, *Phys. Rev. Lett.* **120**, 040407 (2018).
- [49] Z. Liu, E. J. Bergholtz, and E. Kapit, Non-abelian fractional Chern insulators from long-range interactions, *Phys. Rev. B* **88**, 205101 (2013).
- [50] E. Kapit and E. Mueller, Exact parent Hamiltonian for the quantum Hall states in a lattice, *Phys. Rev. Lett.* **105**, 215303 (2010).
- [51] A. G. Grushin, T. Neupert, C. Chamon, and C. Mudry, Enhancing the stability of a fractional Chern insulator against competing phases, *Phys. Rev. B* **86**, 205125 (2012).
- [52] Z. Liu, E. J. Bergholtz, H. Fan, and A. M. Läuchli, Fractional Chern insulators in topological flat bands with higher Chern number, *Phys. Rev. Lett.* **109**, 186805 (2012).
- [53] M. Gonçalves, B. Amorim, E. V. Castro, and P. Ribeiro, Hidden dualities in 1D quasiperiodic lattice models, *SciPost Physics* **13**, 046 (2022).

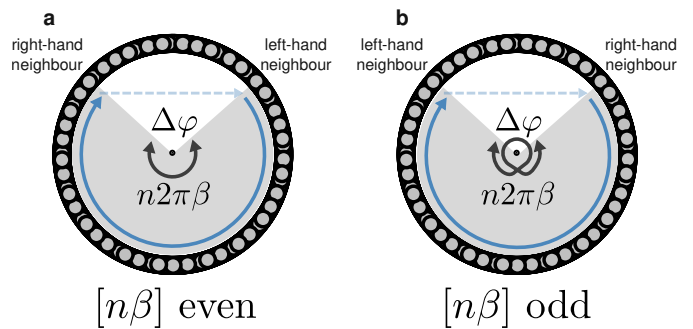


FIG. 7. **Dependence of the signs of the gap labels on the parity of $[n\beta]$:** (a) When $[n\beta]$ is even, the associated Landau-Zener transition involves transport from the right-hand resonant neighbor to the left-hand one. The resulting quantized current flows in the negative direction is therefore associated with a negative Chern number. (b) When $[n\beta]$ is odd, the situation is reversed, and the quantized current, which flows in the positive direction, must be associated with a positive Chern number. Note that in contrast to Fig. 2, we are here considering states below the gap.

Appendix A: Gap labels from perturbation theory

We showed in Section I how resonant pairs of lattice sites coupled by the effective n -th order tunneling element $J_{eff}^{(n)}$ gave rise to pairs of energy gaps in the spectrum of the AAH chain at energies $\pm 2V \cos(n\pi\beta)$. According to the gap labelling theorem, each of these gaps is characterised by a Chern number, whose sign dictates the direction of the current arising under adiabatic pumping when all states below the gap are occupied.

In the case $[n\beta]$ even, let us for instance fill up all states up to the energy $-2V \cos(n\pi\beta)$, see Fig. 7. We note that for the case discussed in Fig. 2 ($n = 1$, $\beta > 0.5$), this energy is positive. For states below this gap, the pumping induces Landau-Zener hoppings in the negative direction, where each Landau-Zener transition transfers the states from the right-hand resonant neighbor to the left-hand one (we can ignore the Landau-Zener processes associated with the gaps below $-2V \cos(n\pi\beta)$, as they do not influence the overall current). This results in a quantized current in the negative direction and this gap is therefore associated with a negative Chern number. The same reasoning can be applied to the state filled up to $2V \cos(n\pi\beta)$, leading to a positive gap label.

In the case $[n\beta]$ odd, the resonant neighbors are flipped, and the adiabatic Landau-Zener transition transfers the states from the left- to the right-hand neighbor. In this case, the quantized current flows in the positive direction and is therefore associated to a positive Chern number.

Therefore, to assign the correct sign to the labels of the energy gaps, one has to treat both the cases of even and odd parity of $n\beta$, as done in Eq. (9).

Appendix B: Critical disorder strengths for first-order bands

We show here how to use the configuration space pictures to derive the critical disorder strength for the 3 bands defined by the $n = \pm 1$ gaps, in the case $\beta > 1/2$. Note that the general idea can be applied to any band, and any value of $\beta > 1/2$. The cases $\beta < 1/2$ can be obtained by sending $\beta \rightarrow 1 - \beta$ and inverting the sign of all Chern numbers.

Let us consider 3 nearest neighbors, which we label with indices $i = -1, 0, 1$, each of them being offset by an onsite disorder of strength w_i . The resonance condition for the -1 and 0 sites is given by

$$2V \cos(\varphi_{-1,0}) + w_{-1} = 2V \cos(\varphi_{-1,0} + 2\pi\beta) + w_0, \quad (\text{B1})$$

while the resonant condition between sites 0 and 1 is given by

$$2V \cos(\varphi_{0,1}) + w_0 = 2V \cos(\varphi_{0,1} + 2\pi\beta) + w_1 \quad (\text{B2})$$

The shifted resonance conditions $\varphi_{-1,0}$ and $\varphi_{0,1}$ can thus be written as:

$$\varphi_{-1,0} = \pi(1 - \beta) + \arcsin\left(\frac{w_0 - w_{-1}}{4V \sin(\pi\beta)}\right) \quad (\text{B3})$$

$$\varphi_{0,1} = -\pi(1 - \beta) + \arcsin\left(\frac{w_1 - w_0}{4V \sin(\pi\beta)}\right) \quad (\text{B4})$$

As discussed in Section III, the breakdown of quantized transport occurs once $\Delta\varphi = \varphi_{-1,0} - \varphi_{0,1} = 0$. For bounded local disorder this becomes possible as soon as the disorder is strong enough to shift the individual resonances to $\varphi_{-1,0} = \varphi_{0,1} = 0$. This condition leads to the following critical disorder strength for the top and bottom $C = +1$ bands:

$$W_{crit}^{C=+1} = 2V \sin^2(\pi\beta). \quad (\text{B5})$$

The same reasoning can be applied to the middle $C = -2$ band, with the only difference that breakdown happens when the resonant angles meet halfway at $\varphi_{left} = \varphi_{right} = \pi/2$, leading to a different critical disorder strength

$$\begin{aligned} W_{crit}^{C=-2} &= 2V |\sin(\pi\beta) \cos(\pi\beta)| \\ &= 2V |\sin(2\pi\beta)|/2 \end{aligned} \quad (\text{B6})$$

We stress that these expressions do not depend on the tunneling strength J , and hence do not depend on the size of the gaps. This explains the stability of the quantized current for disorder strengths that are larger than the size of the clean gaps.

In addition, we note that the same reasoning can be used to derive the critical disorder strength for different kinds of bounded spatial disorder. For instance, in the presence of random phase disorder in onsite energies

of the form $\epsilon_i = 2V \cos(2\pi\beta i + \varphi + W_i)$, the above argument can be directly transposed to conclude that the critical disorder strength required to break the quantized pumping of a given band is directly proportional to the angle (and hence the number of states) in that band:

$$W_{crit}^{C=+1} = \pi|1 - \beta| \quad (\text{B7})$$

$$W_{crit}^{C=-2} = \pi|\beta - \frac{1}{2}| \quad (\text{B8})$$

In both cases, the topological protection increases with the *number of states* in the considered energy bands of the clean system and does not rely on a spectral gap condition, which is in stark contrast with the usual intuition of gap-protected topological properties.

Appendix C: Critical disorder strengths for second-order central band

The perturbation analysis from Eq. (B5) can be extended to second order by looking for the hybridisation of pairs of resonant next-nearest neighbors, mediated by an effective tunneling amplitude (given by $J_{eff}^{(2)} \propto J^2/V$). The corresponding resonance condition is given by:

$$\cos\theta^{(2)} = \cos(\theta^{(2)} + 4\pi\beta), \quad (\text{C1})$$

which causes the opening of two gaps of size $\Delta E^{(2)}/\propto J^2/V$, at energies $E^{(\pm 2)} = \pm 2V \cos 4\pi\beta$. These resonances, combined with the first order resonances, split the spectrum in 5 second-order bands (Fig. 1 c). If the pumping rate is sufficiently slow to allow adiabatic hoppings between next-nearest neighbors, the Thouless pump becomes sensitive to these smaller gaps.

The critical disorder strength required to perturb the quantized current in the $C = +4$ band can be deduced using the argument shown in Fig. 4, with the angles corresponding to the $C = +4$ band. In this case, the angle spanned by the band in configuration space is twice $\Delta\varphi^{C=+4} = 2\pi(\frac{3}{4} - \beta)$. Let us consider 3 next nearest neighbors, labelled $-1, 0, 1$. The disorder can shift these resonance by (at most) an angle:

$$\varphi_{-1,0} = 2\pi(1 - \beta) + \arcsin\left(\frac{w_0 - w_{-1}}{4V \sin(2\pi\beta)}\right) \quad (\text{C2})$$

$$\varphi_{0,1} = -2\pi(1 - \beta) + \arcsin\left(\frac{w_1 - w_0}{4V \sin(2\pi\beta)}\right) \quad (\text{C3})$$

which leads to a breakdown of the quantized current when the resonances meet at $\varphi = \pi/2$, at the critical disorder strength

$$W_{crit}^{C=+4} = 2V |\sin(2\pi\beta) \cos(2\pi\beta)|, \quad (\text{C4})$$

which shows excellent agreement with numerical simulations (Fig. 3 j).